

# Spin-orbiton and quantum criticality in FeSc<sub>2</sub>S<sub>4</sub>

L. Mittelstädt,<sup>1</sup> M. Schmidt,<sup>1</sup> Zhe Wang,<sup>1</sup> F. Mayr,<sup>1</sup> V. Tsurkan,<sup>1,2</sup> P. Lunkenheimer,<sup>1\*</sup>  
D. Ish<sup>4</sup>, L. Balents,<sup>3</sup> J. Deisenhofer<sup>1</sup>, and A. Loidl<sup>1</sup>

<sup>1</sup>*Experimental Physics V, Center for Electronic Correlations and Magnetism, University of Augsburg, 86135 Augsburg, Germany*

<sup>2</sup>*Institute of Applied Physics, Academy of Sciences of Moldova, MD-2028 Chisinau, Republic of Moldova*

<sup>3</sup>*Kavli Institute for Theoretical Physics, University of California, Santa Barbara, California, 93106-4030, USA*

<sup>4</sup>*Physics Department, University of California, Santa Barbara, California, 93106-4030, USA*

In FeSc<sub>2</sub>S<sub>4</sub>, spin-orbital exchange and strong spin-orbit coupling compete and, hence, this material represents a rare example of a spin-orbital liquid ground state. Moreover, it is close to a quantum-critical point separating the ordered and disordered regimes. Using THz and FIR spectroscopy, we provide clear evidence for a *spin-orbiton* in this material, an excitation of strongly entangled spins and orbitals. It becomes particularly well pronounced upon cooling, when advancing deep into the quantum-critical regime. Moreover, indications of an underlying structureless excitation band are found, a possible signature of quantum criticality.

PACS numbers: 71.70.Ej, 78.30.Hv, 75.40.Gb

In frustrated magnets, conventional long-range magnetic order is suppressed via competing interactions or geometrical frustration. In three dimensions, pyrochlore lattices are the strongest contenders with exotic ground states like spin ice or spin liquids. The diamond lattice is another prominent example: It consists of two interpenetrating fcc lattices and frustration occurs with respect to the ratio of inter- and intra-lattice magnetic exchange. The spinel MnSc<sub>2</sub>S<sub>4</sub>, with manganese at the *A* site forming a diamond lattice and nonmagnetic Sc at the *B* site, is an illuminating example where a spiral spin-liquid state evolves at low temperatures [1,2]. However, not only the spins but also the orbital degrees of freedom can evade long-range order. In FeSc<sub>2</sub>S<sub>4</sub>, Fe<sup>2+</sup> with a d<sup>6</sup> electronic configuration is tetrahedrally coordinated by S<sup>2-</sup>, and consequently reveals a twofold orbital degeneracy. A Jahn-Teller transition leading to long-range orbital order is expected at low temperatures. However, FeSc<sub>2</sub>S<sub>4</sub> neither shows orbital nor magnetic order down to 50 mK, despite a natural energy scale set by the magnetic exchange of 45 K [3]. Hence, it represents one of the rare examples of a spin-orbital liquid (SOL) [3,4,5]. An anomalously small excitation gap in this material was identified by NMR [6] and neutron scattering [7].

Interestingly, based on theoretical considerations, it has been suggested that the SOL state in FeSc<sub>2</sub>S<sub>4</sub> does not result from frustration but from a competition between on-site spin-orbit coupling (SOC) and spin-orbital exchange [4,8,9]. Generally, the coupling of electronic spin and orbital momentum is of prime importance in atomic physics, plays a significant role in condensed matter [10], and even can be used in spin-orbitronics: the simultaneous manipulation of both these electronic degrees of freedom [11,12]. While spin and orbital exchange favors order, strong SOC can result in a SOL state with high entanglement of the spin and orbital subsystems [4,9]. According to this theory, FeSc<sub>2</sub>S<sub>4</sub> is close to a quantum-critical (QC) point between the SOL state and a magnetically and orbitally ordered phase (see inset of Fig. 1).

Quantum criticality provides a new organizing principle in condensed matter physics and can control sizable regions of phase diagrams with far-reaching consequences, including a plethora of exotic phases [13]. Here we present THz- and far-infrared (FIR) spectroscopy results for FeSc<sub>2</sub>S<sub>4</sub> to search for the theoretically predicted generic excitations of SOLs [4,9], which we term spin-orbitons, and for signatures of the QC state. Pure orbital excitations, so-called orbitons, have been observed earlier in orbitally ordered LaMnO<sub>3</sub> (Ref. 14) and vanadium oxides [15]. These crystal-field derived excitations are located in the infrared region while in the present work we focus on the ground-state splitting due to spin-orbit coupling at much lower energies, in the THz regime.

Ceramic samples of FeSc<sub>2</sub>S<sub>4</sub> were prepared as described in the Supplemental Material [16]. Time-domain THz transmission experiments were carried out using a TPS Spectra 3000 spectrometer (TeraView Ltd.). Reflectivity experiments in the FIR range were performed using a Bruker Fourier-transform spectrometer IFS 113v. More details are provided in the Supplemental Material [16].

Figure 1(a) shows the dielectric loss from THz spectroscopy for selected temperatures between 4 and 70 K. Strikingly, at low temperatures a sharp excitation close to 35 cm<sup>-1</sup> evolves from a nearly structureless continuum. We ascribe this mode to a spin-orbiton, an excitation of strongly entangled spin and orbital degrees of freedom [4,8]. For temperatures  $\geq 20$  K, this excitation is rather smeared out and almost overdamped. However, at lower temperatures its eigenfrequencies significantly shift towards higher wave numbers and the damping strongly decreases. At frequencies  $> 40$  cm<sup>-1</sup> and the lowest temperatures, the loss increases more strongly, possibly indicating the appearance of a second excitation (see discussion of Fig. 3 below). For a deeper analysis, the data were fitted by the sum of a Lorentzian line shape and an increasing background, the latter estimated by a spline interpolation between the regions just outside the excitation peak. The fit curves [lines in Fig. 1(a)] are in good

agreement with experiment. The resulting parameters of the Lorentzian are provided in Figs. 1(b) - (d), all showing significant changes of temperature characteristics below about 17 K (vertical line).

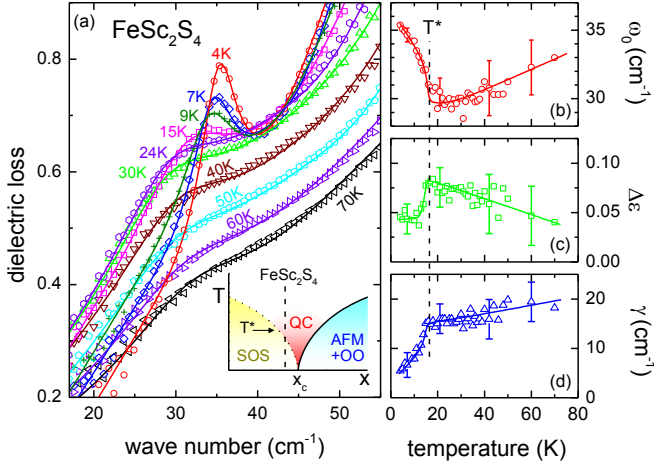


FIG. 1. Temperature dependence of the dielectric loss spectra and the parameters of the lowest spin-orbital excitation. (a) Dielectric loss of  $\text{FeSc}_2\text{S}_4$  at low wave numbers for temperatures between 4 and 70 K. The solid lines represent fits using Lorentzian line shapes including a temperature-dependent background (see text). Right column: Temperature dependence of eigenfrequency (b), of the dielectric strength (c), and of the damping constant (d) of the spin-orbital. The solid lines in (b), (c), and (d) serve as guides to the eye. The dashed vertical line indicates a temperature  $T^* \approx 17$  K, below which a change of the characteristics of the excitation is observed. The inset in (a) shows a schematic phase diagram based on theoretical considerations [4,9], where  $x$  represents the ratio of magnetic exchange  $J$  to the effective spin-orbit interaction  $\lambda = 6\lambda_0^2/\Delta$ , where  $\lambda_0$  is the atomic spin-orbit coupling and  $\Delta$  the crystal-field splitting. A quantum-critical region separates the spin-orbital singlet (SOS) and ordered state, where the latter shows antiferromagnetic (AFM) and orbital order (OO). The vertical dashed line indicates the position of  $\text{FeSc}_2\text{S}_4$ , for which the QC regime is estimated to arise between about 2 and 45 K [4]. The characteristic temperature  $T^*$ , located within the QC regime, is indicated by the arrow.

These findings can directly be compared to model calculations of the SOL in  $\text{FeSc}_2\text{S}_4$ . According to Refs. [4] and [8], SOC splits the local spin and orbital degeneracy to form entangled spin-orbital states, with a spin-orbital singlet ground state. These states in turn are renormalized by exchange, such that the triplet magnetic excitations acquire strong dispersion, being soft close to the zone boundary, corresponding to a wave vector characteristic for hypothetical antiferromagnetic order and with strongly enhanced eigenfrequencies at the zone center. The triplet excitation minimum at the zone boundary is in good agreement with results from neutron scattering [7] and NMR [6]. The modes expected in optical spectra can be deduced from studies of on-site spin-orbital excitations of isolated tetrahedral  $\text{Fe}^{2+}$  [17]. By SOC, the ground state is split into five equidistant energy

levels with a separation of  $\lambda \approx 15 \text{ cm}^{-1}$ , where  $\lambda$  is the effective SOC constant. A magnetic dipole mode is expected at  $\lambda$  and an electric dipole excitation at  $3\lambda$ . According to Ref. [8], the exchange-induced dispersion renormalizes the triplet mode at  $\lambda$  to a maximum at the zone center of approximately  $1.9\lambda$ . While the renormalization of the electric excitation has not been studied theoretically, some upward shift is also expected at zero momentum.

Comparing the evolution of a well-defined excitation close to  $35 \text{ cm}^{-1}$  in Fig. 1(a) to the theoretical estimate of  $\approx 30 \text{ cm}^{-1}$  gives confidence to its interpretation in terms of a renormalized magnetic dipole excitation. Interestingly, the eigenfrequencies of this excitation significantly increase and its damping decreases below  $T^* \approx 17$  K [Figs. 1(b) - (d)], i.e. within the QC region (inset of Fig. 1), which was estimated to emerge between about 2 and 45 K [4]. This change of temperature characteristics is consistent with the formation of the SOL state and most likely signals the gradual loss of decay channels as one advances deeper into the QC regime.

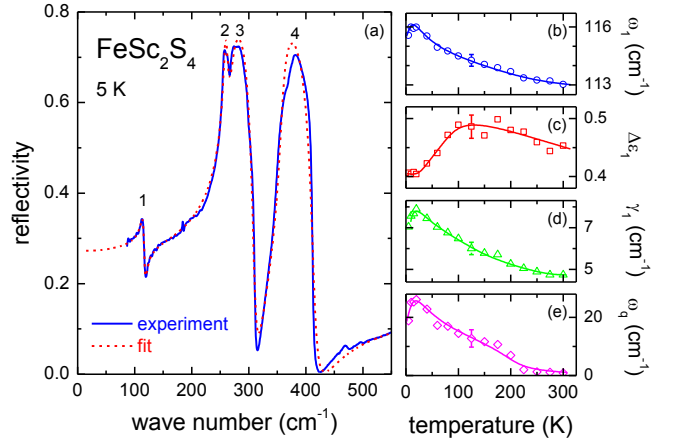


FIG. 2. FIR reflectivity of  $\text{FeSc}_2\text{S}_4$ . (a) FIR measurements between 80 and  $600 \text{ cm}^{-1}$  are compared with a fit utilizing four Lorentz oscillators. The four phonon modes are indexed from 1 to 4. The right frames show the temperature dependence of eigenfrequency  $\omega_0$  (b), dielectric strength  $\Delta\epsilon$  (c), damping  $\gamma$  (d), and the Fano factor  $\omega_q$  (e) of phonon 1 close to  $115 \text{ cm}^{-1}$ . In (b) to (e), typical error bars are indicated. The solid lines are drawn to guide the eye.

Figure 2 shows the reflectivity of  $\text{FeSc}_2\text{S}_4$  in the FIR region at 5 K. It is fitted assuming four Lorentz oscillators characterizing the four optical phonons expected for normal spinel compounds. Phonon 1, close to  $115 \text{ cm}^{-1}$ , can only be satisfactorily described assuming an asymmetric Fano-type line shape as resulting from interference of resonant scattering with a broad excitation continuum [18] (see Supplemental Material [16]). A reasonable agreement of fits [19] and experimental data is achieved in this way (Fig. 2). A corresponding analysis was performed for various temperatures up to 300 K, yielding temperature-dependent eigenfrequencies, oscillator strengths, damping constants, and (for phonon 1) the Fano factor. Phonon modes 2-4 show

temperature-dependent parameters, typical for canonical anharmonic modes (see Supplemental Material [16]). However, for the phonon mode at  $115 \text{ cm}^{-1}$  the eigenfrequency [Fig. 2(b)] shows no sign of saturation at low temperatures and the damping constant [Fig. 2(d)] significantly increases on decreasing temperature, both contrary to canonical behavior. Most interestingly, the oscillator strength of this mode [Fig. 2(c)] exhibits a slight increase from room temperature down to 100 K, but then decreases by almost 20 % upon further cooling. It seems reasonable that some optical weight is transferred to the low-frequency spin-orbital excitations. Indeed, at least some fraction of the optical weight reappears in the spin-orbital: A comparison of Figs. 1(c) and 2(c) reveals that the phonon loses 0.1 in optical strength while the spin-orbital itself has a dielectric strength of the order of 0.05. Obviously, a large fraction of the optical weight is also transferred into the continuum or in a possible second excitation. The Fano factor [Fig. 2(e)] approaches zero at high temperatures but becomes large at low temperatures. Notably, the temperature dependences of all parameters reveal anomalies close to 15-20 K. They correspond to the variations in the spin-orbital excitation below about 17 K, documented in Fig. 1.

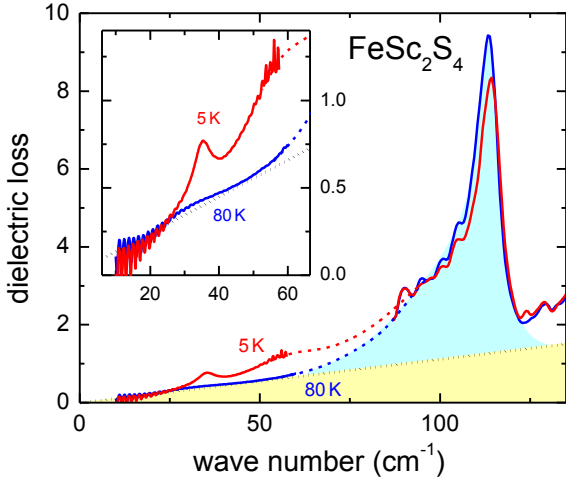


FIG. 3. Low-frequency dielectric loss of  $\text{FeSc}_2\text{S}_4$ . Combined THz and FIR results of the dielectric loss for wave numbers between 10 and  $135 \text{ cm}^{-1}$ , covering spin-orbital excitations and the lowest phonon mode. The results at 5 K are compared to measurements at 80 K. The high-temperature spectrum is composed of a linear excitation continuum (yellow) and a Fano-type phonon mode (blue). As revealed by the inset, showing a magnified view of the low-frequency results, a heavily damped spin-orbital mode is superimposed to the continuum. At 5 K, excess intensity is observed, consistent with a spin-orbital emerging from a superlinear background. The dashed lines are guides for the eyes.

Further significant information can be obtained from Fig. 3 showing the combined THz and FIR loss spectra at 5 and 80 K: i) At 80 K, an almost linear increase at frequencies below  $60 \text{ cm}^{-1}$  forms a continuum below the spin-orbital

excitation peak. In contrast, at 5 K a stronger superlinear background is found. ii) Phonon mode 1 has a strongly asymmetric Fano line shape, in agreement with the fits of the reflectivity. It can be assumed to arise from interference of the resonant lattice vibration with the continuum of the SOL discussed in the following paragraph. iii) The optical weight of the phonon mode at  $115 \text{ cm}^{-1}$  becomes suppressed at low temperatures [cf. Fig. 2(c)] and obviously is partly transferred to the spin-orbital excitation. iv) At 5 K and frequencies beyond the first spin-orbital peak, significant excess intensity emerges. Interestingly, just in this spectral region (at frequencies higher than  $3\lambda = 45 \text{ cm}^{-1}$ ) the presence of a second spin-orbital excitation is theoretically predicted as discussed above. However, at present it cannot be excluded that this excess intensity arises from the mentioned superlinear background and/or from the Fano-type low-frequency wing of the phonon mode. Only future experimental work, closing the frequency gap between about 60 and  $85 \text{ cm}^{-1}$ , can provide a definite proof of a possible second spin-orbital in this region.

The presence of continuum weight in the optical conductivity is actually an expected signature of quantum criticality, which induces scale invariant power-law behavior of many physical properties. In  $\text{FeSc}_2\text{S}_4$  at high temperatures, the dielectric loss clearly exhibits an underlying linear increase in frequency. According to theory, in the QC regime the SOL is described by a multi-component  $\phi^4$  theory, where  $\phi_a$  are the components of the antiferromagnetic order parameter [4,8]. To determine the contribution of QC modes to the dielectric constant, we require the relation of the electric polarization  $P_a$  to the order parameter. With some reasonable assumptions, a symmetry analysis implies  $P_a \propto C_{abcd} \phi_b \partial_c \phi_d$ , where  $C$  is a non-zero tensor. Then the contribution to the dielectric constant is  $\Delta\epsilon \propto \langle P(\omega) P(-\omega) \rangle$ . This correlation function can be calculated following standard methods [20], which gives  $\epsilon''(\omega) \propto \omega^2 \coth(\omega/4k_B T)$ , where  $k_B$  is Boltzmann's constant, for frequencies well above the gap. Physically, the continuum arises due to the contribution of pairs of triplet excitations. Note that the above form is only strictly valid when  $\omega$  is small compared to the magnetic bandwidth, but it nevertheless qualitatively explains the linear dielectric background found at high temperatures elegantly. Moreover, for low temperatures the coth factor becomes constant leading to a superlinear increase, in accord with the experimental findings (Fig. 3). However, it should be noted that the experimentally observed temperature dependence of the continuum is not well reproduced by theory as the coth term (assuming a temperature-independent prefactor) decreases with decreasing temperature.

In summary, we have clearly identified a low-lying spin-orbital excitation in  $\text{FeSc}_2\text{S}_4$ , termed spin-orbital, which strongly couples to phonon excitations. Moreover, a temperature-dependent underlying background contribution to the dielectric loss seems to indicate a spin-orbital excitation continuum, a characteristic signature of quantum criticality [4,8]. The spin-orbital changes character below  $T^* \approx 17 \text{ K}$ , deep within the QC regime, which may indicate an

unexpected fine structure of decay channels. Explaining this finding represents a challenge for future theoretical and experimental exploration.

We thank N. P. Armitage for helpful comments. This work was supported by the Deutsche Forschungsgemeinschaft via the Transregional Collaborative Research Center TRR 80. D.I. and L.B. were supported by the U.S. D.O.E. grant DE-FG02-08ER46524.

---

\* Corresponding author.

peter.lunkenheimer@physik.uni-augsburg.de

- [1] D. Bergmann, J. H. Alicea, E. Gull, S. Trebst, and L. Balents, *Nature Phys.* **3**, 487 (2007).
- [2] A. Krimmel, M. Müksch, V. Tsurkan, M. M. Koza, H. Mutka, C. Ritter, D. V. Shetyakov, S. Horn, and A. Loidl, *Phys. Rev. B* **73**, 014413 (2006).
- [3] V. Fritsch, J. Hemberger, N. Büttgen, E.-W. Scheidt, H.-A. Krug von Nidda, A. Loidl, and V. Tsurkan, *Phys. Rev. Lett.* **92**, 116401 (2004).
- [4] G. Chen, L. Balents, and A. P. Schnyder, *Phys. Rev. Lett.* **102**, 096406 (2009).
- [5] S. Nakatsuji, K. Kuga, K. Kimura, R. Satake, N. Katayama, E. Nishibori, H. Sawa, R. Ishii, M. Hagiwara, F. Bridges, T. U. Ito, W. Higemoto, Y. Karaki, M. Halim, A. A. Nugroho, J. A. Rodriguez-Rivera, M. A. Green, and C. Broholm, *Science* **336**, 559 (2012).
- [6] N. Büttgen, A. Zymara, C. Kegler, V. Tsurkan, and A. Loidl, *Phys. Rev. B* **73**, 132409 (2006).
- [7] A. Krimmel, M. Müksch, V. Tsurkan, M. M. Koza, H. Mutka, and A. Loidl, *Phys. Rev. Lett.* **94**, 237402 (2005).
- [8] G. Chen, A. P. Schnyder, and L. Balents, *Phys. Rev. B* **80**, 224409 (2009).
- [9] K. Balents, *Nature* **464**, 199 (2010).
- [10] Y. Tokura and N. Nagaosa, *Science* **288**, 462 (2000).
- [11] H. Kurebayashi, J. Sinova, D. Fang, A. C. Irvine, T. D. Skinner, J. Wunderlich, V. Novák, R. P. Campion, B. L. Gallagher, E. K. Vehstedt, L. P. Zárbo, K. Výborný, A. J. Ferguson, and T. Jungwirth, *Nature Nanotech.* **9**, 211 (2014).
- [12] A. Manchon, *Nat. Phys.* **10**, 340 (2014).
- [13] P. Coleman and A. J. Schofield, *Nature* **433**, 226 (2005).
- [14] E. Saitoh, S. Okamoto, K. T. Takahashi, K. Tobe, K. Yamamoto, T. Kimura, S. Ishihara, S. Maekawa, and Y. Tokura, *Nature* **410**, 180 (2001); see also the existing controversy about the interpretation of these results: M. Grüninger, R. Rückamp, M. Windt, P. Reutler, C. Zobel, T. Lorenz, A. Freimuth, and A. Revcolevschi, *Nature* **418**, 39 (2002); E. Saitoh, S. Okamoto, K. Tobe, K. Yamamoto, T. Kimura, S. Ishihara, S. Maekawa, and Y. Tokura, *Nature* **418**, 40 (2002).
- [15] S. Miyasaka, S. Onoda, Y. Okimoto, J. Fujioka, M. Iwama, N. Nagaosa, and Y. Tokura, *Phys. Rev. Lett.* **94**, 076405 (2005).
- [16] See Supplemental Material for further results from THz spectroscopy, an analysis of the FIR reflectivity spectra, and more experimental details.
- [17] G. A. Slack, S. Roberts, and F. S. Ham, *Phys. Rev.* **155**, 170 (1967).
- [18] U. Fano, *Phys. Rev.* **124**, 1866 (1961).
- [19] A. Kuzmenko, *RefFIT* v1.2.91, University of Geneva, <http://optics.unige.ch/alexey/refit.html>.
- [20] K. Damle and S. Sachdev, *Phys. Rev. B* **56**, 8714 (1997).

# Supplemental Material

## Spin-orbiton and quantum criticality in $\text{FeSc}_2\text{S}_4$

L. Mittelstädt,<sup>1</sup> M. Schmidt,<sup>1</sup> Zhe Wang,<sup>1</sup> F. Mayr,<sup>1</sup> V. Tsurkan,<sup>1,2</sup> P. Lunkenheimer,<sup>1,\*</sup>  
D. Ish<sup>4</sup>, L. Balents<sup>3</sup>, J. Deisenhofer<sup>1</sup>, and A. Loidl<sup>1</sup>

<sup>1</sup>Experimental Physics V, Center for Electronic Correlations and Magnetism, University of Augsburg, 86135 Augsburg, Germany

<sup>2</sup>Institute of Applied Physics, Academy of Sciences of Moldova, MD-2028 Chisinau, Republic of Moldova

<sup>3</sup>Kavli Institute for Theoretical Physics, University of California, Santa Barbara, California, 93106-4030, USA

<sup>4</sup>Physics Department, University of California, Santa Barbara, California, 93106-4030, USA

\*e-mail: peter.lunkenheimer@physik.uni-augsburg.de

This supplemental material to the manuscript *Spin-orbiton and quantum criticality in  $\text{FeSc}_2\text{S}_4$*  provides detailed information on the results from THz spectroscopy and on the analysis of FIR reflectivity spectra using Lorentzian oscillators including Fano-like line shapes. In addition, further experimental details are provided.

### 1. THz spectroscopy

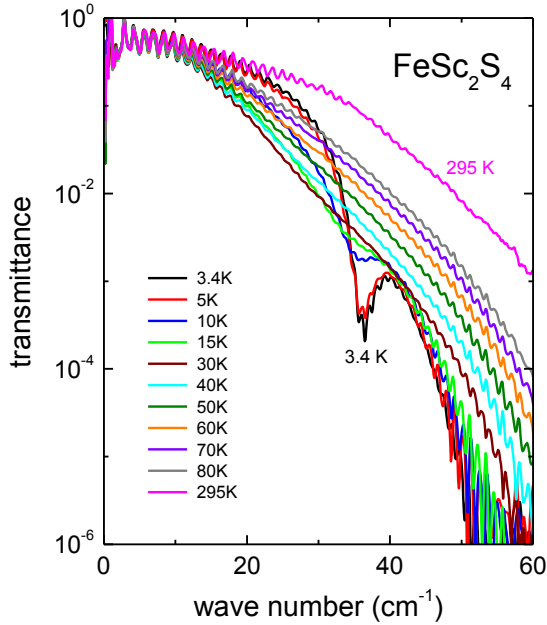


FIG. S1. THz Transmittance of  $\text{FeSc}_2\text{S}_4$ . Transmittance on a logarithmic scale as function of wave numbers up to  $60 \text{ cm}^{-1}$  for room temperature, compared to a series of temperatures between 3.4 and 80 K in the spin-orbital liquid state.

Figure S1 shows the THz transmittance as measured for wave numbers between some  $\text{cm}^{-1}$  up to  $60 \text{ cm}^{-1}$  and temperatures  $3.4 \text{ K} < T < 80 \text{ K}$ . The room-temperature transmittance is included for comparison. All spectra are modulated by interference patterns which become strongly enhanced at low and high wave numbers. They result from multiple reflections in the cryostat windows and from the

sample and cannot be fully removed even by a detailed and advanced analysis including Fresnel optical formulas for reflectance and transmittance. Despite these experimental limitations, two remarkable facts can be clearly identified: i) At low temperatures an excitation evolves close to  $30\text{-}35 \text{ cm}^{-1}$ . Below about 15 K, it starts to shift to higher frequency and its damping is significantly reduced. For  $T > 50 \text{ K}$  this excitation is either overdamped or has lost its dielectric oscillator weight. ii) While at  $10 \text{ cm}^{-1}$  the transmittance remains almost temperature independent, at  $50 \text{ cm}^{-1}$  the transmittance decreases by more than three orders of magnitude between room and liquid-helium temperature which makes it almost impossible to cover a large frequency regime by a single experimental set up. iii) It is also interesting to note how the transmittance close to  $20 \text{ cm}^{-1}$  increases again below 80 K and almost reaches the room temperature value at 3.4 K. This enormous and non-continuous temperature dependence of the absorbance at this wave number range far below the phonon eigenfrequencies documents the strong coupling of spin-orbital excitations to electromagnetic radiation. The lowest-frequency phonon mode appears close to  $115 \text{ cm}^{-1}$  and cannot explain the strong decrease in transmittance on decreasing temperatures.

For a closer analysis, the measured THz spectra, transmittance and phase shift, were converted into a wave-number dependence of the complex dielectric constant. In Fig. S2 we show the dielectric loss for selected temperatures between 4 and 70 K in a color-coded contour plot. These data have been taken on the same polycrystalline sample with the same thickness of 1.15 mm as those shown in Fig. S1, but were measured with different window configurations, to avoid interference noise close to the excitation frequencies, but also to prove reproducibility of the THz results, specifically the linear increase of dielectric loss corresponding to a excitation continuum of the spin orbital liquid. In Fig. S2 the evolution of a well-defined excitation close to  $35 \text{ cm}^{-1}$  is clearly visible. The eigenfrequencies shift

towards low wave numbers and reveal a strongly decreasing damping below about 15-20 K. The spin-orbital excitation appears on top of an almost linearly increasing background. The color code above Figure S2 indicates this linear background, with a dielectric loss which is zero at zero wave number and has been set to 0.8 at 65  $\text{cm}^{-1}$ . The code pattern is very close to the frequency dependence of the loss at 70 K indicating that indeed at this temperature the loss increases strictly linearly. The enhancement of the loss at large wave numbers and low temperatures indicates the appearance of a second mode outside of the covered frequency window.

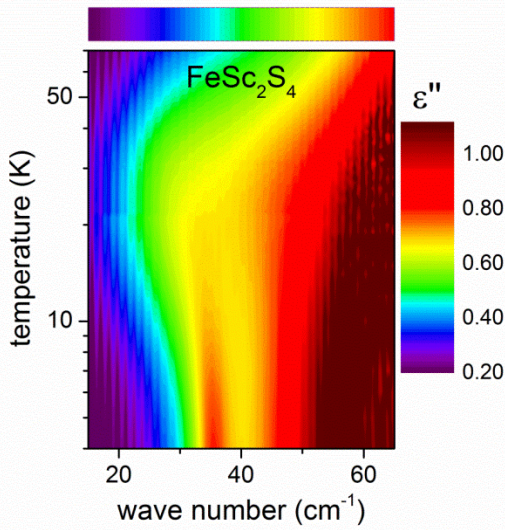


FIG. S2. Color coded contour plot of the dielectric loss of  $\text{FeSc}_2\text{S}_4$ . The dielectric loss is plotted vs. the logarithm of temperature ( $4 \text{ K} < T < 70 \text{ K}$ ) and vs. wave number between 15 and 65  $\text{cm}^{-1}$  in a linear color code as indicated on the right side of Figure S2. The upper bar on top of the figure indicates a strictly linear increase of the loss with wave number.

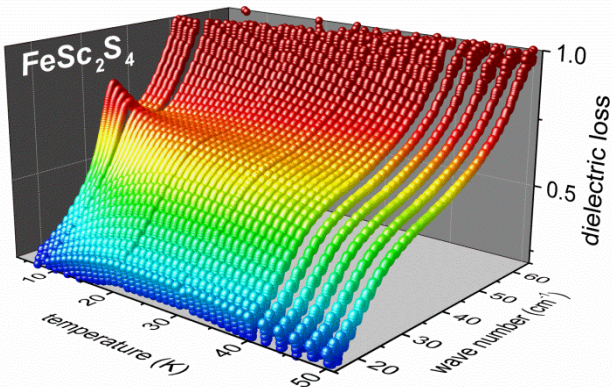


FIG. S3. Three dimensional plot of the dielectric loss of  $\text{FeSc}_2\text{S}_4$  vs. wave number and temperature. The loss is color coded to indicate equal-loss contours above the temperature wave-number plane.

Figure S3 shows the same data in a three-dimensional plot of the dielectric loss. This figure more clearly shows how the spin-orbital excitation evolves from a structureless continuum with linear energy dependence. Moreover, it strikingly documents how below about 15-20 K this excitation becomes exceedingly sharper and shifts to higher frequency below a temperature  $T^* \approx 17 \text{ K}$ , within the quantum-critical regime. For higher temperatures, this excitation becomes smeared out and almost overdamped. A closer inspection of Fig. S3 again reveals that at the lowest temperatures, while the loss at low frequencies becomes suppressed, at higher frequencies it becomes enhanced indicating the appearance of a second spin-orbital excitation.

## 2. FIR spectroscopy

A representative result of the reflectivity as observed in  $\text{FeSc}_2\text{S}_4$  for wave numbers between 80 and 550  $\text{cm}^{-1}$  is shown in the main paper in Fig. 2(a). Room-temperature FIR spectra of  $\text{FeSc}_2\text{S}_4$  have been published previously with so far unexplained five IR-active phonon excitations<sup>1</sup>. Our results as documented in Fig. 2(a) reveal four prominent reflectivity bands, characteristic for normal spinel compounds<sup>2</sup>. The narrow spike close to 180  $\text{cm}^{-1}$  is an experimental artefact and the weak mode close to 470  $\text{cm}^{-1}$ , earlier interpreted as phonon mode<sup>1</sup>, could be the reflectance due an electronic quadrupolar excitation<sup>3</sup> but is not further analyzed in the course of this work. The experimental reflectivity is fitted assuming four Lorentz oscillators characterizing the four optical phonons expected for normal spinel compounds. We found out that phonon mode 1 close to 115  $\text{cm}^{-1}$  can only be satisfactorily described assuming a Fano-type line shape. An asymmetric Fano line shape results from interference of resonant scattering with a broad excitation continuum and is a common phenomenon in atomic and solid state physics<sup>4</sup>. Adapting this Fano-type phenomenon for the formalism of the complex dielectric constant derived from a Lorentz oscillator gives

$$\epsilon(\omega) = \frac{\omega_p^2}{\omega_0^2 - \omega^2 - i\gamma\omega} \left(1 + i \frac{\omega_q}{\omega}\right)^2 + \left(\frac{\omega_p\omega_q}{\omega_0\omega}\right)^2 \quad (1)$$

Here  $\omega_0$  is the phonon eigenfrequency,  $\omega_p$  is the ionic plasma frequency,  $\gamma$  the damping constant of the phonon modes, describing the inverse life time of phonon excitations, and  $\omega_q$  is the Fano factor describing the asymmetry of the phonon line shape. From the ionic plasma frequency, the dielectric strength  $\Delta\epsilon = (\omega_p/\omega_0)^2$  can be calculated. The influence of the Fano parameter  $\omega_q$  on the frequency dependence of the dielectric loss is shown in Fig. S4 for a series of Fano parameters. It is clear from eq. (1) that for  $\omega_q = 0$  the Lorentzian line shape is recovered.

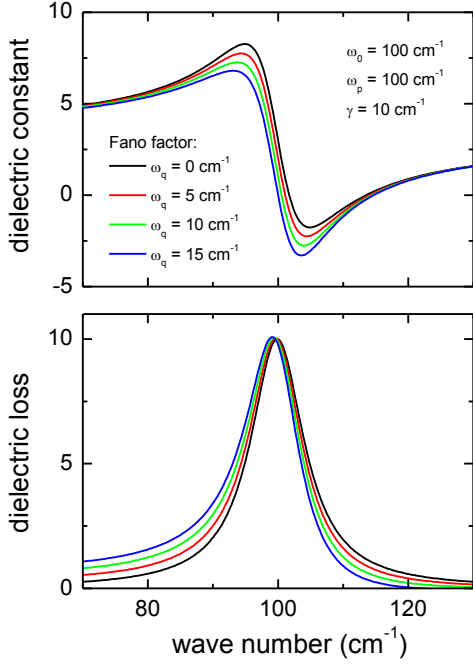


FIG. S4. Dielectric constant and loss calculated with different strengths of the Fano parameter. The complex dielectric constant is calculated for a model phonon as indicated in the upper frame using eq. (1) with different strengths of the Fano factor  $\omega_q$ .

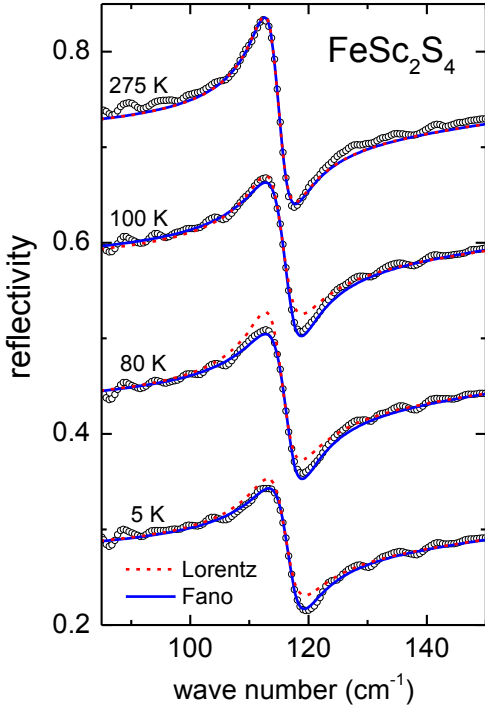


FIG. S5. Temperature dependence of the reflectivity in  $\text{FeSc}_2\text{S}_4$ . For clarity reasons, the reflectivity curves for 80, 100 and 275 K are shifted upwards. The reflectivity of phonon mode 1 of  $\text{FeSc}_2\text{S}_4$  was fitted with a pure Lorentz oscillator model (dashed red lines) or with a Fano resonance model, eq. (1) (solid blue lines).

The present reflectivity results can be satisfactorily described utilizing a fit routine developed by Kuzmenko, where Fano effects have been recently included<sup>5</sup>. We have fitted the reflectivity of  $\text{FeSc}_2\text{S}_4$  utilizing this fit routine. We found that reasonable fits can only be obtained including a temperature-dependent Fano factor for the lowest phonon mode (phonon 1). While below 100 K the strong asymmetry can only be described including a rather large Fano factor, the fits close to room temperature are hardly improved and reasonable fits can be obtained utilizing Lorentzian line shapes. This is documented in Fig. S5 for the lowest phonon mode close to  $115 \text{ cm}^{-1}$ . Here we show representative results of the reflectivity and the importance of the Fano factor  $\omega_q$  for a series of temperatures.

Utilizing this fit routine, the experimentally obtained reflectivity spectra for wavenumbers between 80 and  $550 \text{ cm}^{-1}$  were fitted for all temperatures. Eigenfrequency  $\omega_0$ , damping  $\gamma$ , and oscillator strength  $\Delta\epsilon$  were used as free fit parameters for each phonon mode. As outlined above, the Fano factor  $\omega_q$  was added to the Lorentzian oscillator and was treated as fit parameter for phonon mode 1. In addition, the high-frequency dielectric constant  $\epsilon_\infty$  was also treated as free parameter. As documented in Fig. 2 of the main paper for the reflectivity at 5 K, a reasonable agreement of fit<sup>5</sup> and experimental data could be achieved in this way. Even at the lowest temperatures we found no indications of a splitting of phonon modes due to antiferromagnetic exchange, which is a universal feature for antiferromagnetic compounds<sup>6</sup>. From these fits we determined eigenfrequencies, dipolar strengths and damping constants for all four modes and, in addition for phonon 1, the Fano factor. The fit parameters eigenfrequency  $\omega_0$ , damping  $\gamma$ , oscillator strength  $\Delta\epsilon$ , and Fano factor  $\omega_q$  were determined for phonon mode 1 for all temperatures. The results are shown in the main manuscript in Figs. 2(b) - (e). For the modes 2 - 4, the temperature dependencies of eigenfrequencies, oscillator strength, and damping are documented in Fig. S6.

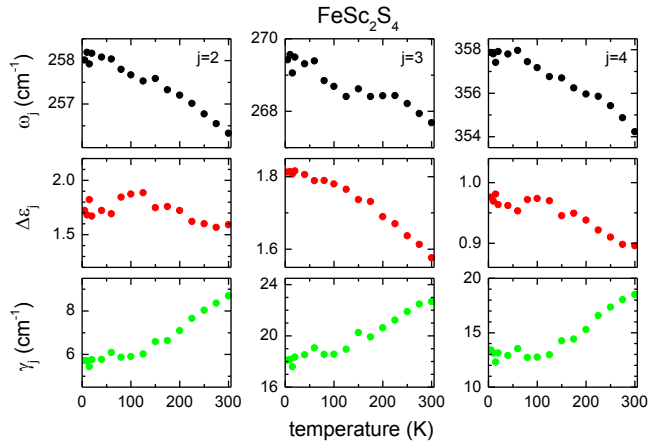


FIG. S6. Eigenfrequencies, oscillator strength, and damping of phonon modes 2 - 4 in  $\text{FeSc}_2\text{S}_4$  as function of temperature.

The temperature dependence of eigenfrequencies and damping of these modes behave conventional, like in moderately anharmonic solids: The eigenfrequencies approach constant values at low temperatures (low compared to an overall Debye temperature) and decrease linearly on increasing temperatures, which mainly results from thermal expansion effects. The damping is low and constant at low temperatures and increases linearly on increasing temperatures. The oscillator strength is expected to be constant and temperature independent. We see continuous shifts of order 5%, which seem to be outside of experimental uncertainties and remain unexplained. They could only be explained assuming valence changes of the ions, which, however, seem rather unlikely in the strictly insulating material.

From the fits we also determined the temperature dependence of the high-frequency dielectric constant  $\epsilon_\infty$ . As documented in Fig. S7, it is only weakly temperature dependent and of order 5.  $\epsilon_\infty$  and the sum over all four oscillator strengths  $\Delta\epsilon$  determine the temperature dependence of the static dielectric constants  $\epsilon_s$ . As also is documented in Fig. S7, the latter again is only weakly temperature dependent with values close to 10.

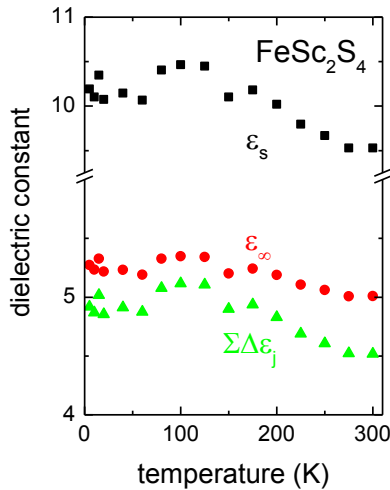


FIG. S7. Temperature dependence of static and high-frequency dielectric constants of  $\text{FeSc}_2\text{S}_4$ .

### 3. Experimental Details

**Sample preparation and characterization.** Samples of  $\text{FeSc}_2\text{S}_4$  were prepared by sintering stoichiometric mixtures of the high-purity elements Fe (4N), Sc (3N) and S (5N) in evacuated sealed silica ampoules at  $1000^\circ\text{C}$ . After a sintering time of one week, the samples were powdered, homogenized, pressed into pellets and annealed again at  $1000^\circ\text{C}$ , a synthesis procedure which was repeated several times to reach full reaction. The samples were characterized by X-ray diffraction, magnetic susceptibility and heat-capacity experiments, resulting in structural, magnetic, and

thermodynamic properties as described in detail by Fritsch et al.<sup>3</sup>

**THz spectroscopy.** Time-domain THz transmission experiments were carried out on polycrystalline samples in the spectral range from  $10 - 100 \text{ cm}^{-1}$  using a TPS Spectra 3000 spectrometer (TeraView Ltd.) on samples with thickness ranging from 0.7 to 1.2 mm and cross sections of the order  $25 \text{ mm}^2$ . Different cryostat windows of quartz glass with thickness of approximately 1 mm and of polypropylene with thickness of  $75 \mu\text{m}$  were utilized. A He-flow cryostat was used to reach the temperatures ranging from 4 - 300 K. Transmission and phase shift were obtained from the Fourier-transformed time-domain signal. Dielectric constant and loss were calculated from transmission and phase shift by modelling the sample as a homogeneous dielectric. Here, for simplicity reasons, we assumed a magnetic permeability of  $\mu = 1$ , which may lead to some ambiguities in the case of purely magnetic contributions to the optical response.

**FIR experiments.** Reflectivity experiments were carried out in the FIR range using the Bruker Fourier-transform spectrometer IFS 113v equipped with a He bath cryostat. With the set of mirrors and detectors used for these experiments, we were able to cover a frequency range from  $60$  to  $700 \text{ cm}^{-1}$ . For the reflectivity experiments, the ceramics were pressed with a maximum pressure of 1 GPa with the surfaces polished to optical quality. Nevertheless, neither surface nor density of the samples was ideal and of perfect optical quality and we were not able to receive reliable results below  $80 \text{ cm}^{-1}$ . In THz spectroscopy, real and imaginary part of the dielectric permittivity can be directly derived from transmission and phase shift. From the THz data, we determined absolute values of the real and imaginary parts of the permittivity. From the FIR reflectivity, the permittivity was calculated via a Kramers-Kronig transformation. We had to correct all FIR reflectivity spectra by a factor of 1.3 to bring in line the permittivity from the FIR and THz results. This correction was necessary to account for low densities and non-ideal surfaces of the ceramic samples. In addition, we produced high-density samples, with large grain size and almost perfect surface quality by spark-plasma sintering. In these samples, we found good agreement with the absolute values of the permittivity as determined by THz spectroscopy. The obtained permittivity was approximately by a factor of 1.3 larger than for the unscaled FIR results of standard ceramic samples, justifying the applied factor. However, in these samples dc-conductivity contributions dominated at low frequencies revealed by THz spectroscopy, probably due to slight off-stoichiometries of sulfur and, hence, considerable doping effects. For the combined data, it seems necessary to use results obtained on the same samples and, hence, in the FIR region the scaled data set is used. All reflectivity spectra were fitted using the RefFIT fit routine<sup>5</sup>, including the option for Fano-type resonance line shapes.

## References

- <sup>1</sup> S. Reil, H.-J. Stork, and H. Haeuseler, *J. Alloys Comp.* **334**, 92 (2002).
- <sup>2</sup> T. Rudolf, Ch. Kant, F. Mayr, J. Hemberger, V. Tsurkan, and A. Loidl, *New J. Phys.* **9**, 76 (2007).
- <sup>3</sup> Ch. Kant, T. Rudolf, F. Schrettle, F. Mayr, J. Deisenhofer, P. Lunkenheimer, M. V. Eremin, and A. Loidl, *Phys. Rev. B* **78**, 245103 (2008).
- <sup>4</sup> U. Fano, *Phys. Rev.* **124**, 1866 (1961).
- <sup>5</sup> A. Kuzmenko, *ReFIT* v1.2.91, University of Geneva, <http://optics.unige.ch/alexey/reffit.html>.
- <sup>6</sup> Ch. Kant, M. Schmidt, Zhe Wang, F. Mayr, V. Tsurkan, J. Deisenhofer, and A. Loidl, *Phys. Rev. Lett.* **108**, 177203 (2012).